16th Australasian Fluid Mechanics Conference
Crown Plaza, Gold Coast, Australia
2-7 December 2007

Evidence of large-scale amplitude modulation on the near-wall turbulence

R. Mathis, N. Hutchins and I. Marusic

Walter Basset Aerodynamics Laboratory, Mechanical and Manufacturing Engineering
University of Melbourne, Victoria, 3010 Australia

Abstract

The relationship between large- and small-scale motions remains a poorly understood process in wall-bounded turbulence. Such misunderstanding is perhaps, in part, due to the limited scale separation typical of many laboratory-scale facilities. A recent investigation performed by Hutchins and Marusic [11] in a high Reynolds number turbulent boundary layer has qualitatively shown the existence of a modulating influence of the large-scale log region motions on the small-scale near-wall cycle. For this study we build upon these observations, using the Hilbert transformation applied to the spectrally filtered small-scale component of fluctuating velocity signals, in order to quantitatively determine the degree of amplitude modulation imparted by the large-scale structures onto the near-wall cycle.

Introduction

Over the past several decades, a great many studies have been directed towards understanding the turbulence structure in the near-wall region of wall-bounded flows. To a large extent, such studies have their origins in the observations of Kline *et al.* [16] and the realisation that recurrent near-wall structures can play a key role in turbulence regeneration. More recently our understanding of such events has tended to shift towards a self-sustaining near-wall cycle, in which the near-wall structures propagate and sustain without need of external triggers. Such autonomous views are based largely on insightful low Reynolds number simulations by Jiménez & Pinelli [13] and Schoppa & Hussain [21].

The logarithmic region was largely absent from the earliest low Reynolds number flow visualisations and DNS studies. For example, the approximate upper and lower bounds of the logarithmic region ($100 < z^+ < 0.15\delta^+$), would indicate that almost no overlap region was present in the measurements of Kline *et al.* [16]. However, advances in Particle Image Velocimetry (PIV) and Direct Numerical Simulations (DNS) have afforded the opportunity to study the turbulence structure in the logarithmic region of higher Reynolds turbulent boundary layers (Adrian *et al.* [1], del Álamo *et al.* [2]). PIV studies of streamwise/spanwise planes have revealed the presence of a pronounced stripiness in instantaneous fields of streamwise velocity (u) fluctuation [7, 22, 10]. Such elongated regions of momentum deficit have been explained within vortex based models as the region between the legs of aligned packets of hairpin vortices [1, 7, 22, 10, and others]. These low-speed regions are typically $0.3-0.5\delta$ wide in the spanwise direction, and seem to often occur in spanwise alternating patterns (elongated low-speed events are usually flanked on either side by high speed events). The length of these features often exceeds the streamwise length of the PIV images. Hutchins & Marusic [12] employed rakes of hot-wire probes to ascertain the true length of these structures, demonstrating that they routinely exceed 15δ in length and meander substantially. They used the collective term 'superstructures' to describe these events. Ganapathisubramani *et al.* [6] used a multiple side-by-side arrangement of cameras to image $8\delta \times 2\delta$ streamwise/spanwise planes in a supersonic turbulent boundary layer, finding similar elongated meandering features. For pipe flows, the energetic footprint of superstructure events is evident as low-wavenumber peaks in pre-multiplied energy spectra, termed very large-scale motions or VLSM [14, 8]. More recently Monty *et al.* [20] have employed hot-wire rakes in the log region of both channels and pipes, reiterating the general presence and form of superstructures in internal geometries.

It is natural to consider what effect these very large log region events might have on the near-wall cycle. Use of the term 'autonomous' when referring to the near-wall cycle can tend to negate the influence of larger scales which, although perhaps not strictly a prerequisite for the near-wall cycle, may still impart an influence or modulation on near-wall events. One clear example of such an influence is in the breakdown of universal behaviour based on viscous scaling in the near-wall region. The viscous-scaled near-wall peak in the streamwise broadband intensity clearly grows in magnitude with increasing Reynolds number [15, 5, 19, 18, 17]. Moreover, it has been shown that such growth is due to the increase of large-scale energy imparted onto the near-wall region as Re increases [18, 12, 11]. Hutchins & Marusic clearly show that the footprint of large-scale superstructure events in the streamwise velocity fluctuations can extend deep into the near-wall region [12]. This is as predicted by Townsend [23], who noted that the near-wall region will feel wall-parallel motions due to all attached eddies with centres above that height (right across the shear layer). Thus, in the near-wall, the streamwise velocity fluctuations will be the sum of the induced fluctuations from every scale that resides above (including superstructures). In this instance the large-scale energy is merely superimposed as a low-wavenumber shift onto the near-wall, and by definition (since it is largely wall-parallel), will not contribute to the Reynolds shear stress.

By studying fluctuating velocity signals from hot-wire sensors in the near-wall region, Hutchins and Marusic [11], recently observed that in addition to the low-wavenumber mean shift, the largest scales appeared to be 'amplitude modulating' the small-scale fluctuations. They noted that the large regions of streamwise momentum deficit (associated with the footprint of the 'superstructures') are accompanied by reduced small-scale fluctuations in the near-wall region. On the other hand, for large-scale high-momentum regions, the small-scale fluctuating component is more energetic. They also found that, away from the wall, this scenario seems to reverse, with the more energetic small-scale fluctuations eventually becoming aligned with that part of the superstructure that is in momentum deficit. Bandyopadhyay and Hussain [3] have also looked at the relationship between large- and small-scales in a number of shear flows. They found significant coupling between scales, and also noted the same reversal in coupling occurring across the boundary layer (referring to this as a phase difference).

For the present paper, we expand upon the initial observations of Hutchins and Marusic [11], using the Hilbert transformation

in an attempt to quantify the relationship between large-scale fluctuations and any amplitude modulation of the small-scale energy in turbulent boundary layers. It should be noted throughout that when discussing 'smaller-scales' we are referring to a sub-set of small-scales (in the range $100 \lesssim \lambda_x^+ \lesssim 1000$), and not to the fine-scales also known as the Kolmogorov or dissipation scales.

Experimental data set

The present analysis is performed on a single experimental data set of hot-wire measurements conducted in the high Reynolds number boundary-layer wind-tunnel (HRNBLWT) at the University of Melbourne. The friction Reynolds number $Re_\tau = \delta U_\tau/\nu = 7300$ (where δ is the boundary layer thickness, U_τ is the friction velocity and ν is kinematic viscosity). The hot-wire sensor had a viscous scaled sensing length $l^+ = lU_\tau/\nu = 22$ (where l is the sensor length). The non-dimensional time interval between samples was $T^+ \simeq 0.4$ and the total sample length was in the range of 5000-14000 boundary layer turnover times. Key boundary layer parameters for the hot-wire measurements are summarised in Tab. 1. Further details concerning experimental setup and measurement procedure are given in Hutchins and Marusic [12, 11]. Full details of the wind tunnel facility are provide by Hafez *et al.* [9].

U_τ (m/s)	δ (m)	Re_τ	l (m)	l^+
0.331	0.330	7300	0.001	22

Table 1: Boundary layer characteristics of hot-wire measurements.

Throughout this paper, the coordinate system, x, y and z, refer to the streamwise, spanwise and wall-normal directions. The respective fluctuating velocity components are denoted by u, v and w. The spectral density function of the streamwise velocity fluctuation is described by ϕ_{uu}. Over-bars indicate time-averaged values and the superscript "+" is used to denote viscous scaling of the length $z^+ = zU_\tau/\nu$, velocities $u^+ = u/U_\tau$ and time $t^+ = tU_\tau^2/\nu$.

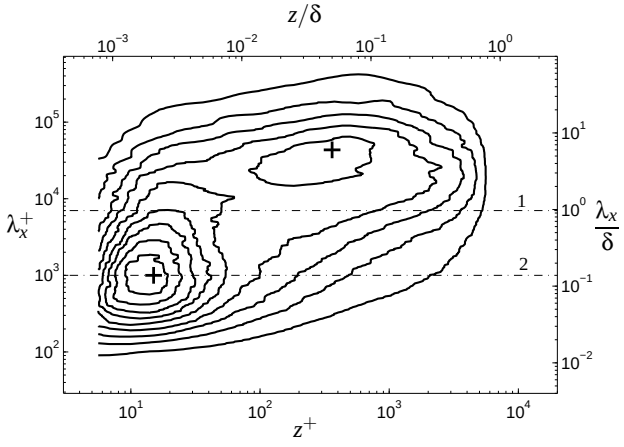

Figure 1: Iso-contours of the pre-multiplied energy spectra of streamwise velocity fluctuation $k_x\phi_{uu}/U_\tau^2$; Contour levels are form 0.2 to 2.0 in steps of 0.2. The large " + " mark the inner peak ($z^+ = 15$, $\lambda_x^+ = 1000$) and the outer peak ($z/\delta = 0.05$, $\lambda_x/\delta = 6$); The horizontal dot-dashed lines show the location of the spectral filters.

Brief review of Hutchins & Marusic [11]

Figure 1 gives an overview of the pre-multiplied streamwise energy spectra, $k_x\phi_{uu}/U_\tau^2$, across the full height of the turbulent boundary layer (where k_x is the streamwise wavenumber). The iso-contours depict the surface formed from the one-dimensional pre-multiplied spectra of u fluctuations at each of the 51 logarithmically spaced measurement stations across the boundary layer. A more detailed explanation of how these energy maps are formed is given by Hutchins & Marusic [12, 11]. It is worth noting that the representation here in terms of streamwise length-scale (λ_x/δ) is only a reflected mirror of the conventional $k_x\phi_{uu}/U_\tau^2$ versus $\log(k_x\delta)$ plot (equal areas under the curve will still denote equal energy).

Two distinct peaks can be clearly observed on figure 1 (the locations of these are marked by the + symbols). The first peak, located in the near-wall region, is the energy signature due to the viscous-scaled near-wall cycle of elongated high- and low-speed streaks (Kline *et al.* [16]). The location of this peak is fixed in viscous coordinates: $z^+ = 15$ and $\lambda^+ = 1000$. We will refer to this peak as the "inner site" in accordance with Hutchins and Marusic [12]. A second distinct peak appears in the logarithmic region. We will refer this peak as the "outer site". The location of this peak appears to scale on boundary layer thickness: $z/\delta = 0.05$ and $\lambda_x = 6\delta$. It is of interest to note that this peak will not be visible at low Reynolds numbers (where $Re_\tau \lesssim 1700$, see [12, 11]) due to insufficient separation of scales. This outer peak is most likely the energetic signature due to the superstructure type events (or VLSM). It has been shown [12] that the magnitude of this peak (when $k_x\phi_{uu}$ is scaled with U_τ) increases with Reynolds number.

Using a decomposition for scales below and above a cutoff length-scale ($\lambda_x^+ = 7300$ and $\lambda_x^+ = 1000$), some interesting features of the signal appear. The dot-dashed lines of Figure 1 show the locations of these cut-offs on the energy map.

subscript	name	spectral filter	
L1	large-scales only	low-pass	$\lambda_x^+ > 7300$
h1	small-scales	high-pass	$\lambda_x^+ < 7300$
h2	smaller-scales	high-pass	$\lambda_x^+ < 1000$

Table 2: Filter parameters and key.

Figure 2 shows such a decomposition of a typical fluctuating signal u^+ at $z^+ = 15$. The original signal (shown in figure 2*a*) is decomposed into three sub-signal parts;

1. the large-scale component u_{L1}^+ which is assumed to be the signature of superstructure-type events (where $\lambda_x^+ > 7300$, figure 2*b*)
2. the small-scale component signal u_{h1}^+ (where $\lambda_x^+ < 7300$, figure 2*c*)
3. and the smaller-scale component signal u_{h2}^+ (where $\lambda_x^+ < 1000$, figure 2*d*)

It is noted that when a negative large-scale fluctuation occurs, the amplitude of the small-scale fluctuations u_{h1}^+ is reduced. This is even more so for u_{h2}^+. It was this result that prompted Hutchins & Marusic to suggest that the low-wavenumber motions associated with superstructure type events in the log region influence the near-wall u fluctuations in a manner akin to a pure amplitude modulation.

We now present a refined analysis based on this observation, attempting to quantify the 'amplitude modulation' effect. Specif-

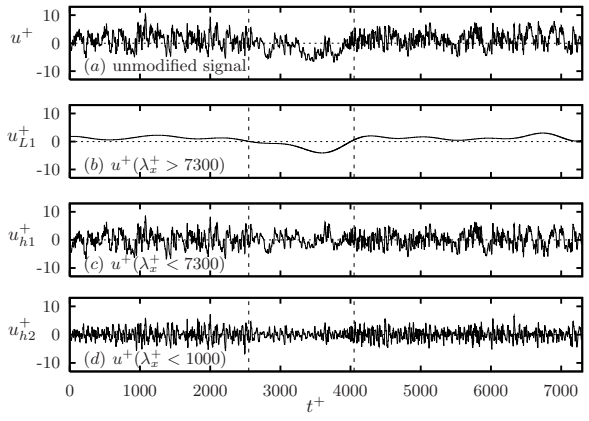

Figure 2: Example of fluctuating u signal in the near-wall region, $z^+ = 15$; (a) raw fluctuating component; (b) large-scale fluctuation $\lambda_x^+ > 7300$; (c) small-scale fluctuation $\lambda_x^+ < 7300$; (d) smaller-scale fluctuation $\lambda_x^+ < 1000$; Dashed vertical lines show region of negative large-scale fluctuation.

ically, we employ the Hilbert transformation to characterise the envelope of the small-scale fluctuations, comparing this to the large-scale filtered signal u_{L1}. The Hilbert transform and its application in demodulating signals is outlined briefly in the following section.

The Hilbert transform and amplitude modulation

For every real-valued signal $x(t)$, it is always possible to determine its Hilbert transformation given by

$$\mathcal{H}\{x(t)\} = \frac{1}{\pi} P \int_{-\infty}^{+\infty} \frac{x(\tau)}{t-\tau} d\tau \tag{1}$$

where P indicates the Cauchy principal value of the integral. $\mathcal{H}\{x(t)\}$ is basically the original signal $x(t)$ with each sinusoidal Fourier component shifted by -90° for positive frequencies, and by $+90^\circ$ for each negative frequency. By this definition, $x(t)$ and $\mathcal{H}\{x(t)\}$ can form a complex conjugate pair,

$$Z(t) = x(t) + i\mathcal{H}\{x(t)\} = A(t)e^{i\phi(t)}. \tag{2}$$

This is an analytic signal (all negative frequencies have been removed). It can be shown (see example given in Appendix 1) that the modulus of this analytic signal,

$$A(t) = \sqrt{x^2(t) + \mathcal{H}\{x(t)\}^2} \tag{3}$$

represents the envelope of the original real-valued signal $x(t)$. As will be seen, this relationship is very useful when attempting to interpret (or demodulate) amplitude modulated signals. A brief tutorial on the Hilbert transform, with emphasis on physical interpretation, can be found in Bendat and Piersol [4].

Amplitude modulation refers to the modulation of a high-frequency signal (carrier signal), with a low-frequency component (modulating signal). The principle is simple: the carrier signal is multiplied by the modulating signal added to some judiciously selected offset B.

The carrier signal could be defined as,

$$c(t) = C\sin(\omega_c t + \phi_c),$$

where C and ϕ_c are arbitrary constants. These constants are here respectively set to values 1 and 0 for simplicity. Figure 3a shows a carrier signal with $\omega_c = 10$. Let us also consider an arbitrary waveform representing the modulating signal,

$$m(t) = M\sin(\omega_m t + \phi_m)$$

where M and ϕ_m are again arbitrary constants also set to 1 and 0 for simplicity (typically $\omega_m < \omega_c$). Figure 3b shows an example modulating signal with $\omega_m = 2$. Amplitude modulation is attained by forming the product

$$u(t) = [B + m(t)]c(t) \tag{4}$$

$$u(t) = [B + \sin(\omega_m)]\sin(\omega_c) \tag{5}$$

where B represents the offset (set to 2 for the present example). The modulation depth M/B indicates the extent to which the modulated variable varies around its original level (in this case C). This must be less than one to ensure a pure amplitude modulated signal. It can be seen that the modulated signal is composed of three Fourier components, a carrier wave (ω_c) and two sinusoidal waves (known as sidebands) whose frequencies are above and below the original carrier wave ($\omega_c - \omega_m$ and $\omega_c + \omega_m$).

The modulus of the analytic signal formed from the Hilbert transformation of $u(t)$ (equation 2), would in this case return the original modulating signal $m(t)$ shifted by the constant B, and is thus invaluable in demodulating amplitude modulated signals.

An example of the modulated signal as given by equation (5) is shown in figure 3c, with a modulation depth of 0.5. The dashed line on figure 3c shows the envelope as calculated from the Hilbert transform, which in this case exactly matches the modulating signal $m(t)$ with the appropriate applied shift B.

From this result, a simple analogy with the results of Hutchins and Marusic [11] can be formulated. If we consider the existence of a modulating effect from the large-scale structures imposed on to the small-scales in the near-wall region, this would imply that the envelope of the high-frequency part of the signal (Figures 2c & 2d) must be directly correlated with the low-frequency part of the signal (Figure 2b). We will introduce in the following section the process used to highlight the coupling between these different scales.

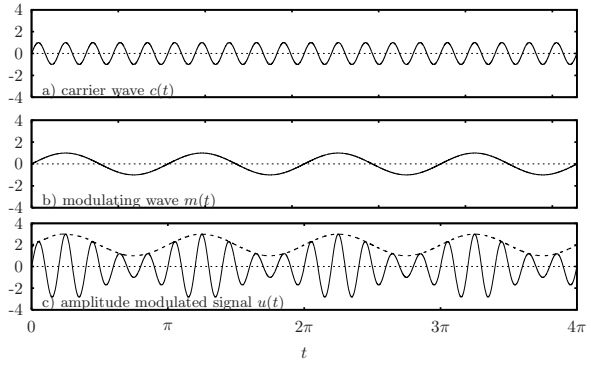

Figure 3: Example of amplitude modulation; (a) represents the carrier wave $c(t) = \sin(10t)$; (b) represents the modulating wave $m(t) = \sin(2t)$; (c) represents the modulated signal $u(t) = [2 + m(t)]c(t)$ (solid line) and its envelope calculated from the Hilbert transform (dashed line).

Coupling process

The coupling between the low- and the high-frequency components of the signal is determined in the following way. From

Figure 1 presented above, the inner site and outer site are clearly separated in wavenumber space. Therefore, a "reasonable" cut-off length-scale for the large-scale motions can be established (we use $\lambda_x^+ = 7300$ in accordance with [11]). A second cutoff length for the smaller-scale motions, $\lambda_x^+ = 1000$, was also selected. This choice was motivated by the assumption that the modulation effect is most discernible in the smaller-scales (figure 2*d*).

The low- and high-frequency parts of the signals were obtained by applying spectral cut-off filters on the raw fluctuating velocity. More specifically, the large- and small-scale components of the signal (u_{L1}^+ and u_{h1}^+ respectively) were obtained by applying respectively a low- and high-pass filter at the cutoff frequency $\lambda_x^+ = 7300$. The smaller-scale component (u_{h2}^+) was obtained by applying a high-pass filter at the cutoff frequency $\lambda_x^+ = 1000$ (see table 2).

In order to determine the relationship between the large- and small-scale structure contained in any velocity signal, the small-scale components of the signal (u_{h1}^+ and u_{h2}^+) were analysed using the Hilbert transformation. The Hilbert transformation allows us to extract the envelope $(E(u_{hi}^+)_{i=1,2})$ of the signal representative of any modulating effect (assumed here to be the large-scale component u_{L1}^+). The obtained envelope is low-pass filtered at the cutoff $L1$ (same as the large-scale). Hence a pseudo-low-frequency envelope $(E_{L1}(u_{hi}^+)_{i=1,2})$ describing the modulation of small- and smaller-scale structures is obtained. It is now possible to compute a meaningful correlation coefficient, R, of this filtered envelope with the large-scale velocity fluctuation u_{L1}^+.

$$R_i = \frac{\overline{u_{L1}^+ \; E_{L1}(u_{hi}^+)}}{\tilde{u}_{L1}^+ \; \tilde{E}_{L1}(u_{hi}^+)} \; , \; i = 1,2 \qquad (6)$$

where tilde denotes the *rms* value of the signal.

The coupling analysis can be summarised as 5 distinct steps:

1. low-pass filter the raw fluctuating velocity u at the cutoff frequency $\lambda_x^+ = 7300 \rightarrow$ large-scale component u_{L1}^+.
2. high-pass filter the raw fluctuating velocity u at the cutoff frequencies $\lambda_x^+ = 7300$ and $\lambda_x^+ = 1000 \rightarrow$ small- and smaller-scale components $u_{hi,\, i=1,2}^+$.
3. Hilbert transform the small- and smaller-scale components $\rightarrow$ envelopes $E(u_{hi}^+)_{i=1,2}$.
4. low-pass filter the envelopes at the cutoff frequency $\lambda_x^+ = 7300 \rightarrow$ filtered envelopes $E_{L1}(u_{hi}^+)_{i=1,2}$.
5. compute the correlation coefficients between the large-scale component and the filtered envelopes $\rightarrow R_{i,\, i=1,2}$.

Results and discussion

An example of the above coupling analysis is first presented for a single measurement station. A more global overview of the modulation, obtained from the application of the analysis across the full height of the boundary layer, is subsequently presented in the final figure.

Coupling process on a sample

The wall-normal location chosen to highlight the principle features of the coupling process is $z^+ = 15$ (corresponding to the 'inner peak' in the pre-multiplied energy spectra due to the near-wall cycle). We will initially use the same short sub-sample as considered by Hutchins and Marusic [11] and considered previously here in figure 2.

The large-scale component u_{L1}^+ for the sample considered here is already given in figure 2*b*.
Figures 4 and 5 present step-by-step the respective results obtained on the small- and smaller-scales decomposition of the signal. Each figure represents, from top to bottom, the three steps of the analysis process required to arrive at the filtered envelope of the small- and smaller-scale components. From the top, the upper plot (*a*) in each case shows the filtered signals u_{h1}^+ and u_{h2}^+ for the respective cutoff length-scales $\lambda_x^+ = 7300$ and $\lambda_x^+ = 1000$. The centre plots (*b*) show the envelopes $E(u_{h1}^+)$ and $E(u_{h2}^+)$ resulting from the Hilbert transformation of the small- and smaller-scale signals. The lower plots (*c*) show the filtered envelopes $E_{L1}(u_{h1}^+)$ and $E_{L1}(u_{h2}^+)$, obtained from low-pass filtering the envelopes at the cutoff $\lambda_x^+ = 7300$. The large-scale component (plus an offset) has been superimposed on plots (*b*) and (*c*) as a dashed line in order to show qualitatively the degree of correlation between the large-scales and the filtered small-scale envelopes (the filtered envelope is amplified by a factor of 2 in order to enhance the reading of the figures).

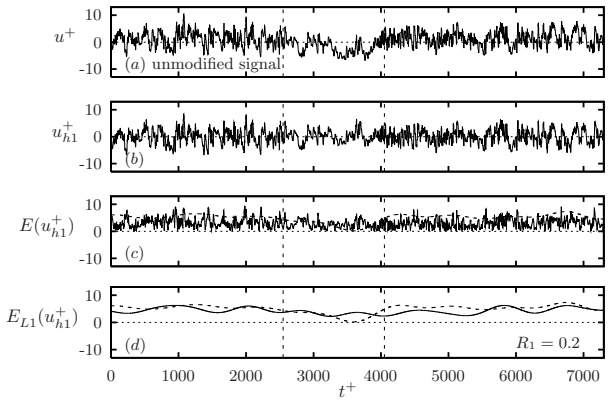

Figure 4: Example of small-scale decomposition on the fluctuating velocity signal at $z^+ = 15$; (*a*) raw fluctuating component; (*b*) the small-scale signal u_{h1}^+ for $\lambda_x^+ < 7300$; (*c*) its envelope $E(u_{h1}^+)$; (*d*) and the filtered envelope $E_{L1}(u_{h1}^+)$. The dashed lines represent the large-scale component u_{L1}^+ shifted by an offset.

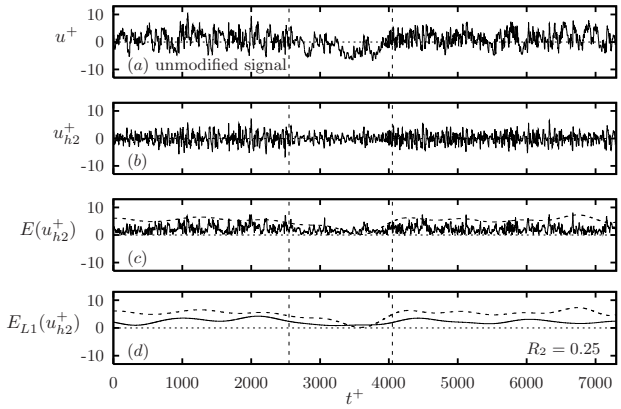

Figure 5: Example of smaller-scale decomposition on the fluctuating velocity signal at $z^+ = 15$; (*a*) raw fluctuating component; (*b*) the smaller-scale signal u_{h2}^+ for $\lambda_x^+ < 1000$; (*c*) its envelope $E(u_{h2}^+)$; (*d*) and the filtered envelope $E_{L1}(u_{h2}^+)$. The dashed lines represent the large-scale component u_{L1}^+ shifted by an offset.

Such qualitative correlations have already been discussed on the filtered signal by Hutchins and Marusic [11]. These observations are here reinforced. Indeed, both the unfiltered and filtered envelopes $E(u_{hi}^+)$ and $E_{L1}(u_{hi}^+)$ (plots (*b*) and (*c*)) exhibit lower fluctuations when the fluctuating large-scale component u_{L1}^+ is negative. This is particularly so for the smaller-scale component (Figure 5) in which the filtered envelope $E_{L1}(u_{h2}^+)$ exhibits a very close approximation to the large-scale component u_{L1}^+. When the large-scale component has a negative fluctuating value (between the vertical dashed lines), the filtered envelope of the smaller-scales show an increasingly flat and lower level. The correlation coefficients R_i between u_{L1}^+ and $E_{L1}^+(u_{hi}^+)$ reach a significant level for both the small- and the smaller-scale components (respectively $R_1 = 0.2$ and $R_2 = 0.25$). This establishes clear quantitative evidence that the large-scale fluctuations, associated with superstructure type events in the log-region, have a measurable and well-defined amplitude modulation effect on the small-scale structures of the near-wall region.

Global evidence of the modulation

The results presented above represent only an instantaneous sub-section of the signal at a single wall-normal location. In order to provide more complete evidence of the amplitude modulation effect, the coupling analysis has been repeated over the entire signal length (480s, representing 5000–14000 boundary layer turn-over times), and for all wall-normal measurement stations. This results in the correlation coefficient $R_i(z^+)_{i=1,2}$, representing the degree of modulation (between the large-scales and the filtered envelope) as a function of wall-normal location.

Prior to discussing the physical significance of the correlation coefficient, it is first necessary to validate the robustness of the the coupling analysis. Due to the number and complexity of the calculations involved in the treatment, it is important to prove that the results are an intrinsic property of the flow and not just some mathematical artifact resulting from the different tools employed. The process is validated on a synthetic signal. The synthetic signal is constructed using the coefficients from the Fourier decomposed real signal, such that each synthetic mode has the same amplitude as the corresponding real mode but with a randomly scrambled phase. In the spectral domain, the phase has been replaced by a randomly generated number within 0 and 2π. Figure 6*a* shows subsections of the real and synthetic signal (left and right hand plots respectively). Note that from a cursory inspection, both signals look very much like turbulent fluctuating *u* velocity signals. This technique produces a synthetic signal with exactly the same energy spectra and turbulence intensity as the original signal yet without any realistic phase information. Figure 6*b* shows the corresponding energy spectra for each of the two signals, which are near identical. By analysing the filtered signals shown in figure 6*c* it is clear that the synthetic signal (right-hand side) does not seem to be exhibiting any signs of amplitude modulation. Indeed if we compare the negative excursions of the large-scale filtered signal (occurring within the dashed vertical lines of plot (*c*)) it is clear that the modulating influence on the smaller-scale signal u_{h2}^+ (lower plot (*c*)), so obvious for the real signal, is completely absent for the phase scrambled case. When this analysis is extended to the full signals at all wall-normal locations (Figure 6*d*), we note that the correlation coefficient $R_i(z^+)_{i=1,2}$ for the synthetic signal exhibits no correlation between large-scale fluctuations and the filtered small-scale envelope. This is in stark contrast to the left-hand plot of figure 6*d*) which shows that, for the real signal, $R_i(z^+)_{i=1,2}$ can return high levels of correlation, and is a strong function of wall-normal position.

The correlation coefficient $R_i(z^+)_{i=1,2}$ obtained for the real signal (figure 6*d*, left) indicates some interesting variation with wall-normal location. A high level of correlation is observed in the viscous layer of the boundary layer, decreasing progressively towards the log-region. This is interpreted as strong evidence that the near-wall cycle associated with the viscous layer is strongly modulated by low wave-number motions associated with the log-region. In the log-region, the correlation decreases progressively to reach a zero value at about $z^+ = 300$, corresponding reasonably well to the position of the outer peak ($z/\delta \approx 0.05 \Leftrightarrow z^+ \approx 365$). This reversal in correlation behaviour is very much as predicted by Hutchins & Marusic [11] who found that the small-scale energy was smaller under negative large-scale fluctuations up to $z^+ \approx 300$, after which a reversal occurred (and the small-scale fluctuations were more energetic under negative large-scale excursions).

Conclusion

The Hilbert transformation when employed with careful spectral filtering has revealed strong supporting evidence to confirm the initial assumptions proposed by Hutchins and Marusic [11]. In this paper it is shown that, in the viscous and buffer layers, the large-scale component is analogous to a modulating signal whilst the small-scale components can be viewed as a modulated signal. This apparent amplitude modulation, imposed by large-scale log region events onto near-wall viscous-scaled structure, has numerous implications to our assumptions concerning turbulent boundary layers. The near-wall cycle, assumed for some time now to be an autonomous process, is shown here to reside under the modulating influence of the large-scale log region events (superstructures). Hutchins and Marusic [11, 12] have demonstrated that as Reynolds number increases the superstructure events will become more and more pronounced, as the outer peak in the pre-multiplied spectra map (Figure 1) becomes increasingly comparable in energy to the inner peak. Thus at higher Reynolds numbers we might expect the amplitude modulation effect documented here to increase. All of this points towards the conclusion that the large-scale structures will play an increasingly important role in high Reynolds number turbulent boundary layers, and could have important implications to active control of turbulence, such as drag reduction or lift enhancement.

Acknowledgements

We acknowledge the support of the Australian Research Council through the Discovery program (DP-0663499) and the Federation Fellowship program (FF0668703). N.H and I.M also acknowledge the David and Lucile Packard Foundation.

Appendix: A note on the Hilbert transformation

We here give a proof to demonstrate that the envelope of a modulated signal can be obtained from the instantaneous amplitude of the Hilbert transform and the original real-valued signal (equation 3)

$$\begin{aligned} \mathcal{H}\{x(t)\} &= (h * x)(t) \\ &= \int_{-\infty}^{\infty} x(\tau) h(t-\tau) d\tau \\ &= \frac{1}{\pi} P \int_{-\infty}^{\infty} \frac{s(\tau)}{t-\tau} d\tau \end{aligned} \tag{7}$$

where

$$h(t) = \frac{1}{\pi t} \tag{8}$$

and considering the integral as a Cauchy principal value (which avoids the singularities at $\tau = t$, and $\tau = \pm\infty$,).

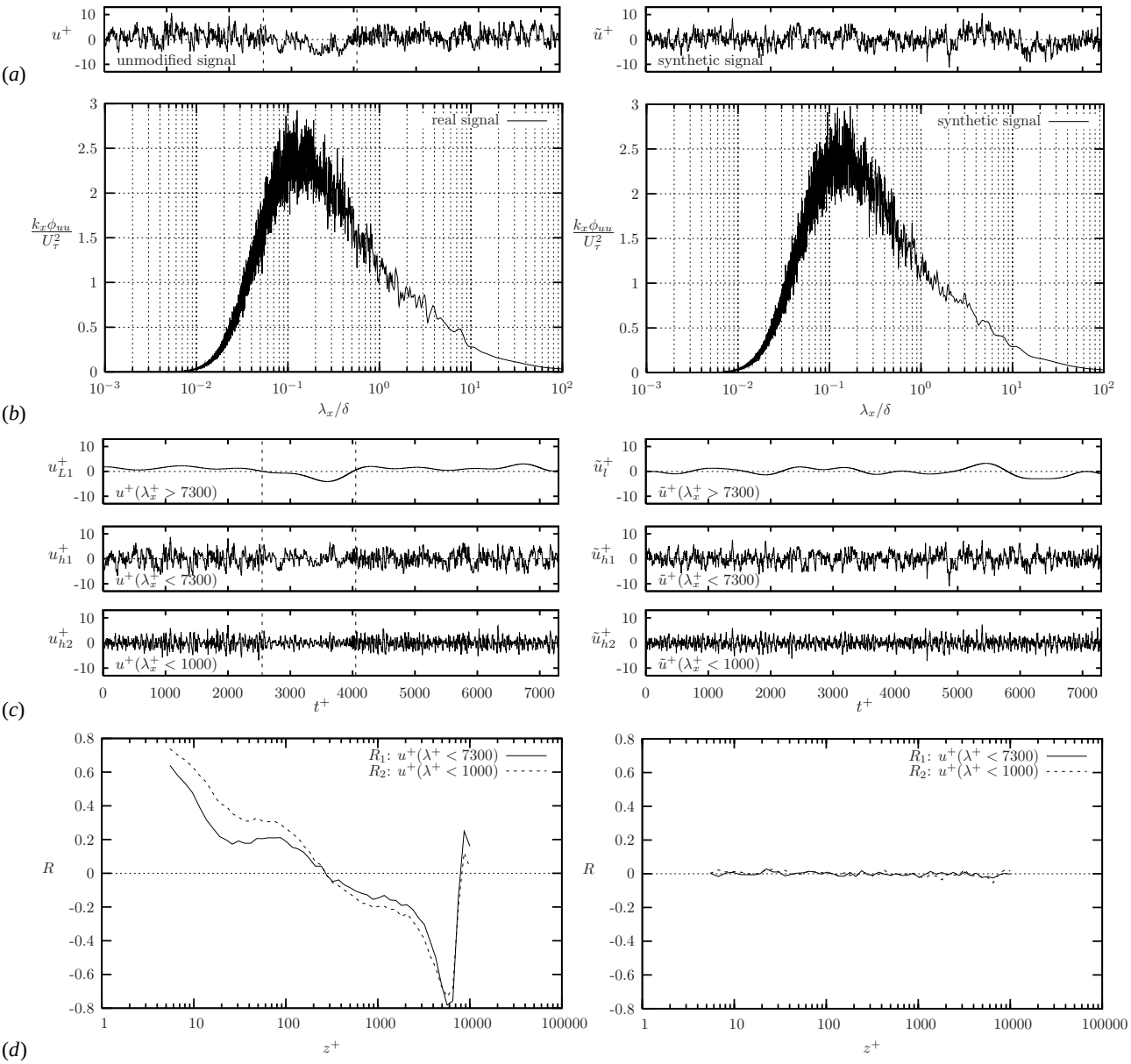

Figure 6: Comparison of the coupling analysis between the real signal (left) and the synthetic phase scrambled signal (right); (*a*) instantaneous sample of raw fluctuating signal; (*b*) pre-multiplied energy spectra; (*c*) large-scale (u_{L1}^+) , small-scale (u_{h1}^+) and smaller-scale (u_{h2}^+) decomposition; (*d*) correlation coefficient $R_i(z^+)_{i=1,2}$ between the large-scale component and the filtered envelope of the (solid) small- and (dashed) smaller-scale component.

Thus, one important property of the Hilbert transformation is

$$\begin{aligned} \mathcal{H}\{\cos(t)\} &= +\sin(t) \\ \mathcal{H}\{\sin(t)\} &= -\cos(t) \end{aligned} \tag{9}$$

Considering a carrier signal (high frequency ω_c)

$$c(t) = C\sin(\omega_c t) \tag{10}$$

and a modulating signal (lower frequency ω_m)

$$m(t) = M\sin(\omega_m t) \tag{11}$$

the amplitude modulated signal is given as

$$u(t) = [B+m(t)]\,c(t) \tag{12}$$

$$\begin{aligned} &= [B+M\sin(\omega_m t)]\,C\sin(\omega_c t) && (13)\\ &= BC\sin(\omega_c t)+MC\sin(\omega_m t)\sin(\omega_c t) \\ &= BC\sin(\omega_c t) && (14)\\ &\quad -\frac{MC}{2}\left(\cos[(\omega_c+\omega_m)t]-\cos[(\omega_c-\omega_m)t]\right) \end{aligned}$$

From this form, it is clear that the modulating signal $u(t)$ has three components: a carrier wave (ω_c) and two additional sinusoidal modes whose frequencies are slightly above and below the carriers wave ($\omega_c-\omega_m$ & $\omega_c+\omega_m$).

The analytic signal of $u(t)$ is defined as

$$L(t) = u(t)+i\mathcal{H}\{u(t)\} = A(t)e^{i(\phi(t))} \tag{15}$$

where the modulus $A(t)$ and the phase $\phi(t)$ are given as

$$A_(t) = \sqrt{u(t)^2 + \mathcal{H}\{u(t)\}^2} \quad (16)$$

$$\phi(t) = \arctan \frac{\mathcal{H}\{u(t)\}}{u(t)} \quad (17)$$

The Hilbert transform can be performed on our amplitude modulated signal $u(t)$ by substituting equation (9) into equation (14).

$$\begin{aligned} \mathcal{H}\{u(t)\} &= -BC\cos(\omega_c t) \\ &\quad -\frac{MC}{2}\left(\sin[(\omega_c+\omega_m)t] - \sin[(\omega_c-\omega_m)t]\right) \\ &= -BC\cos(\omega_c t) - MC\cos(\omega_c t)\sin(\omega_m t) \quad (18) \end{aligned}$$

Substituting (18) and (14) into (16), the modulus $A(t)$ of the Hilbert transformation $\mathcal{H}\{u(t)\}$ can be written as

$$\begin{aligned} A(t) &= [B^2C^2\sin^2(\omega_c t) + 2BMC^2\sin^2(\omega_c t)\sin(\omega_m t) \\ &\quad + M^2C^2\sin^2(\omega_m t)\sin^2(\omega_c t) + B^2C^2\cos^2(\omega_c t) \\ &\quad + 2BMC^2\cos^2(\omega_c t)\sin(\omega_m t) \quad (19) \\ &\quad + M^2C^2\cos^2(\omega_c t)\sin^2(\omega_m t)]^{\frac{1}{2}} \\ &= [B^2C^2 + 2BMC^2\sin(\omega_m t) + M^2C^2\sin^2(\omega_m t)]^{\frac{1}{2}} \\ &= [B + M\sin(\omega_m t)]C \quad (20) \\ &= [B + m(t)]C \quad (21) \end{aligned}$$

i.e. the amplitude of the Hilbert transformation returns the modulating signal, plus a D.C. component, multiplied by the amplitude of the carrier wave.

References

[1] Adrian, R. J., Meinhart, C. D. and Tomkins, C. D., Vortex organization in the outer region of the turbulent boundary layer, *J.Fluid Mech.*, **422**, 2000, 1–54.

[2] del Álamo, J. C., Jiménez, J., Zandonade, P. and Moser, R. D., Scaling of the energy spectra of turbulent channels, *J. Fluid Mech.*, **500**, 2004, 135–144.

[3] Bandyopadhyay, P. R. and Hussain, A. K. M. F., The coupling between scales in shear flows, *Phys. Fluids*, **27** 9, 1984, 2221–2228.

[4] Bendat, J. S. and Piersol, A. G., Random data: Analysis and Measurements Procedures, *New York: Wiley & Sons 2nd ed.*, 1986.

[5] DeGraaff, D. B. & Eaton, J. K., Reynolds number scaling of the flat-plate turbulent boundary layer, *J. Fluid Mech.*, **422**, 2000, 319–346.

[6] Ganapathisubramani, B., Clemens, N. T. & Dolling, D. S., Large-scale motions in a supersonic boundary layer., *J. Fluid Mech.*, **556**, 2006, 271–282.

[7] Ganapathisubramani, B., Longmire, E. K. & Marusic, I.,Characteristics of vortex packets in turbulent boundary layers., *J. Fluid Mech.*, **478**, 2003, 35–46.

[8] Guala, M., Hommema, S. E. & Adrian, R. J., Large-scale and very-large-scale motions in turbulent pipe flow, *J. Fluid Mech.*, **554**, 2006, 521–542.

[9] Hafez, S., Chong, M. S., Marusic, I. and Jones, M. B., Observations on high Reynolds number turbulent boundary layer measurements, In *Proc. 15th Australasian Fluid Mech. Conf.* (ed. M. Behnia, W. Lin & G.D. McBain), Paper AFMC 00200, University of Sydney, 2004.

[10] Hambleton, W. T., Hutchins, N and Marusic, I., Simultaneous orthogonal-plane particular image velocimetry measurements in turbulent boundary layer, *J. Fluid Mech.*, **560**, 2005, 53–64.

[11] Hutchins, N. and Marusic, I., Large-scale influences in near-wall turbulence, *Phil. Trans. R. Soc. A*, **365**, 2007, 647–664.

[12] Hutchins, N. and Marusic, I., Evidence of very long meandering features in the logarithmic region of turbulent boundary layers, *J. Fluid Mech.*, **579**, 2007, 1–28.

[13] Jiménez, J. & Pinelli, A., The autonomous cycle of near-wall turbulence. *J. Fluid Mech.* **389**, 1999, 335–359.

[14] Kim, K. C. & Adrian, R., Very large-scale motion in the outer layer, *Phys. Fluids*, **11**, 1999, 417–422.

[15] Klewicki, J. C. & Falco, R. E., On accurately measuring statistics associated with small-scale structure in turbulent boundary layers using hot-wire probes, *J. Fluid Mech.*, **219**, 1990, 119–142.

[16] Kline, S. J., Reynolds, W. C., Schraub, F. A. and Rundstadler, P. W., The structure of turbulent boundary layers, *J. Fluid Mech.*, **30**, 1967, 741–773.

[17] Marusic, I. & Kunkel, G. J., Streamwise turbulence intensity formulation for flat-plate boundary layers, *Phys. Fluids*, **15**, 2003, 2461–2464.

[18] Metzger, M. M. & Klewicki, J. C., A comparative study of near-wall turbulence in high and low Reynolds number boundary layers, *Phys. Fluids*, **13**, 2001.

[19] Metzger, M. M., Klewicki, J. C., Bradshaw, K. L. & Sadr, R., Scaling the near-wall axial turbulent stress in the zero pressure gradient boundary layer, *Phys. Fluids*, **13, 6**, 2001, 1819–1821.

[20] Monty, J. P., Stewart, J. A., Williams, R. C. & Chong, M. S., Large-scale features in turbulent pipe and channel flows., *J. Fluid Mech.*, 2007, In Press.

[21] Schoppa, W. & Hussain, F.,Coherent structure generation in near-wall turbulence. *J. Fluid Mech.*, **453**, 2002, 57–108.

[22] Tomkins, C. D. & Adrian, R. J., 2003, Spanwise structure and scale growth in turbulent boundary layers, *J. Fluid Mech.*, **490**, 2003, 37–74.

[23] Townsend, A. A., The Structure of Turbulent Shear Flow, *Cambridge University Press*, 1976.